

INFLUENCE OF STRONG SPANWISE MAGNETIC FIELD ON THE QUASI-TWO-DIMENSIONAL MHD FLOW IN A 180-DEGREE SHARP BEND

Azan M. SAPARDI^{1,2}, Wisam K. HUSSAM¹, Alban POTHÉRAT³ and Gregory J. SHEARD^{1,*}

¹ The Sheard Lab, Mechanical and Aerospace Engineering Department, Monash University, Victoria 3800, AUSTRALIA

² Mechanical Engineering Department, Kuliyyah of Engineering, International Islamic University Malaysia, Kuala Lumpur 53300, MALAYSIA

³ Applied Mathematics Research Centre, Coventry University, Coventry CV1 5FB, UNITED KINGDOM

*Corresponding author, E-mail address: Greg.Sheard@monash.edu

ABSTRACT

The quasi-two-dimensional flow of a liquid metal exposed to a strong spanwise magnetic field around a 180-degree sharp bend is investigated using a high-order spectral-element algorithm. This study identifies the effect of strong spanwise magnetic field strength defined by Hartmann number on flow characteristics such as the length of the downstream recirculation bubbles and the threshold Reynolds numbers between steady-state and unsteady flow regimes for the ratio between the width of the bend and the height of the inlet duct, $0.2 \leq \beta \leq 2$. The study reveals that the first recirculation bubble length decreases with increasing Hartmann number. The flow was found to be more stable as observed from the increase of critical Reynolds number for transition from steady to unsteady flow as Hartmann number increases for all β . This study gives useful insight into the generation of instability for improved mixing and heat transport in heat exchanger ducting in MHD systems.

NOMENCLATURE

μ	dynamic viscosity
ρ	density
σ_e	electrical conductivity
a	characteristic length
B	magnetic field strength
H	Hartmann parameter
Ha	Hartmann number
L_{R1}	primary bubble length
L_{R2}	secondary bubble length
L_z	domain length in magnetic field direction
N	interaction parameter
n	number of Hartmann wall
p	pressure
U_o	maximum inlet velocity

INTRODUCTION

The flow of electrically conducting liquid in a duct with the presence of a strong magnetic field underpins in many engineering applications such as metallurgical processing, blood meters and magnetic confinement fusion reactor cooling. The main motivation of this study is the implication of this interaction in magnetic confinement fusion cooling blanket used to transfer heat from the hot plasma fuel in the fusion reactor. The motion of liquid that

is perpendicular to the direction of the magnetic field induces an eddy current, which in turn interacts with the magnetic field producing an electromagnetic Lorentz force opposes to the motion of the fluid. In a small time scale, the Lorentz force acts to redistribute the angular momentum in a single vortex, which makes it preserved in the direction parallel to the magnetic field. Consequently, this compels the flow to become two-dimensional by suppressing secondary flow parallel to the direction of the magnetic field. At larger time-scale, Hartmann damping acts to put a braking force onto the bulk flow velocity which tends to flatten the velocity profile in the duct. The quasi-two-dimensional flow may be efficiently simulated using the quasi-two-dimensional model proposed by Sommeria and Moreau (Sommeria and Moreau, 1982, Pothérat *et al.*, 2000, Pothérat *et al.*, 2005, Hamid *et al.*, 2015).

This 180-degree sharp bend geometry is a key component of the coolant conduits within blankets of magnetic confinement fusion reactors. The working fluid is a liquid metal alloy, and the channels are exposed to a strong magnetic field that significantly alters the flow from the hydrodynamic case (Barleon *et al.*, 1991, Barleon *et al.*, 1996, Boccaccini *et al.*, 2004). According to Kirillov *et al.* (1995), the efficiency of heat transfer in the fusion reactor that involves a huge amount of heat may decrease dramatically due to the strong magnetic field that damps the fluctuations of the flow. The sudden geometry change of the sharp bend creates flow separation which has the potential to enhance the heat transfer process (Sparrow *et al.*, 1987, Liou *et al.*, 1998, Hirota *et al.*, 1999, Astarita and Cardone, 2000, Liou *et al.*, 2000, Chung *et al.*, 2003). However, further investigation is needed to understand the effect of Hartmann braking on the flow to elucidate the demotion of heat transfer efficiency in the metal fluid flow under strong magnetic field effect.

This problem is computed using a two-dimensional spectral-element incompressible flow solver augmented with the linear Hartmann friction term to satisfy the quasi-two-dimensional model. The two-dimensional steady flow structure in the downstream duct is found to have resemblance with the flow over a backward facing step. The flow first passes over a large recirculation bubble attached to the inner wall downstream of the sharp bend, and subsequently another recirculation develops at the outer wall further downstream.

NUMERICAL METHODOLOGY

Viscous fluid is considered flowing in a duct with a sharp 180-degree bend with the origin of our Cartesian coordinate system located at the centre of the inner vertical wall of the bend. The upstream and downstream ducts are parallel to each other. We consider an incompressible flow in this sharp bend.

Figure 1 shows the domain including the geometric parameters considered in this study. a and b represent the height of the inlet and the width of the bend opening, respectively. c denotes the thickness of the divider. Consistent with Zhang and Poth erat (2013), the lengths of the bottom and top boundaries are represented by d and e , respectively. The inlet and outlet height are identical. The ratio of the divider thickness to the inlet height is set to be $c/a = 0.04$. The lengths of the bottom and top boundaries are $d = 15a+b$ and $e = 3d$, respectively. The length of the top boundary is set to be adequately long to capture the dynamics of the flow at the downstream of the sharp bend.

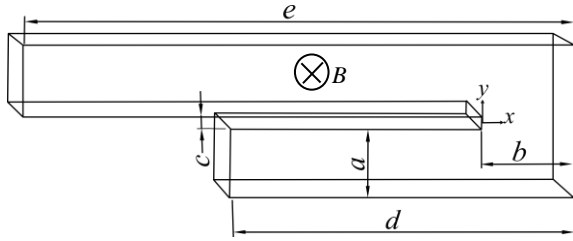


Figure 1: Schematic diagram of geometry. Magnetic field B direction is in the spanwise direction.

Three independent non-dimensional numbers may be used to characterize these quasi-two-dimensional MHD flows. First the Reynolds number,

$$Re = U_o a / \nu, \quad (1)$$

where a is the characteristic length, U_o is the maximum inlet velocity, and ν is the kinematic viscosity of the fluid. Second is Hartmann number, which is the square root of the ratio of Lorentz forces to viscous forces,

$$Ha = L_z B \sqrt{\frac{\sigma_e}{\rho \nu}}, \quad (2)$$

and the third is the interaction parameter, which is the ratio of Lorentz forces to inertia,

$$N = \frac{\sigma_e B^2 L_z^2}{\rho U_o a}. \quad (3)$$

Here L_z , σ_e , ρ and B are the domain length in the direction of the magnetic field, electrical conductivity, mass density and the magnetic field strength, respectively. The interaction parameter can also be interpreted in terms of Ha and Re as $N = Ha^2/Re$. Due to large Ha and N values in magnetic confinement fusion applications, the flow is quasi-2D with a core region where the velocity is constant along the magnetic field direction, and thin Hartmann layers at the walls perpendicular to the magnetic field direction. Under these assumptions, Sommeria and Moreau (Sommeria and Moreau, 1982) have derived a 2-D flow model by averaging the flow equations along the direction of the magnetic field,

$$\frac{\partial \mathbf{u}}{\partial t} = -(\mathbf{u} \cdot \nabla) \mathbf{u} - \nabla p + \frac{1}{Re} \nabla^2 \mathbf{u} - \frac{H}{Re} \mathbf{u}, \quad (4)$$

$$\nabla \cdot \mathbf{u} = 0, \quad (5)$$

where \mathbf{u} is the velocity averaged across the duct along the magnetic field and p is the static pressure. The parameter $H = n(a^2/L_z^2)L_z \sqrt{\sigma_e/(\rho \nu)}$ is a measure of the friction term representing the Lorentz force effect on the flow, n represents the number of Hartmann layers in any given cross-section of the duct, which is in this case $n = 2$.

Velocity is zero at the interface between the wall and the fluid due to viscosity, hence a no-slip boundary condition ($\mathbf{u} = 0$) is imposed. At the outlet boundary ($x = b-e$, $-1.02a \leq y \leq 1.02a$), a standard boundary condition is specified by setting a reference pressure value $p = 0$.

At the inlet boundary ($x = b-d$, $-1.02a \leq y \leq 1.02a$), analytic velocity profile for fully developed laminar duct flow as shown in figure 2 has been imposed. This velocity profile reverts to the Poiseuille velocity profile as H approaches zero which represents non-MHD flow. The velocity profile becomes almost flat at high H except near the adjacent no-slip walls where Shercliff boundary layer with the thickness of $\delta_{Sh} \sim 1/H^{1/2}$ are located.

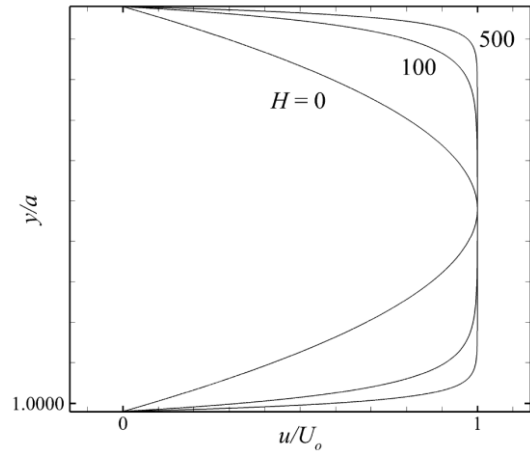


Figure 2: Quasi-two-dimensional velocity profile at H as indicated normalized with maximum inlet velocity for fully developed duct flow.

COMPUTATIONAL METHODS

Polynomial Degree Study

Flow around a 180-degree sharp bend is tremendously difficult to fully resolve, especially at large Re . A grid resolution study was performed to validate the numerical algorithm and to select appropriate meshes and element order in order to get a good optimal solution and computing time. The spatial resolution study varied the order of interpolation within each macro element of a mesh on domain length parameters from the mesh domain.

The mesh is structured and refined in the vicinity of the inner wall of the sharp bend and in the downstream channel as shown in figure 3 in order to capture the intricate structure of the downstream flow. Computations have been performed with polynomial degrees varying from $N = 4$ to 8.

Table 1 demonstrates the accuracy of the primary recirculation bubble length in the base flow computation as a function of polynomial order. The recirculation bubble length was calculated at $Re = 500$ and $\beta = 1$, steady state and has two recirculation bubbles at the downstream as illustrated in figure 4. Polynomial order

$N = 5$ was chosen to be used hereafter considering the small relative error and moderate computing time.

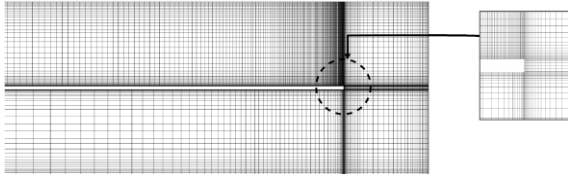


Figure 3: Details of mesh around turning part area with polynomial order $N = 3$.

N	A	B	L_{R1}/a	%diff L_{R1}/a
4	0	-4.80573	4.805727	0.03071
5	0	-4.80716	4.807159	0.00092
6	0	-4.8073	4.807295	0.00192
7	0	-4.80725	4.807248	0.00094
8	0	-4.8072	4.807203	-

Table 1: Dependence of recirculation length on polynomial order. Parameter N indicates the independent polynomial order of the base flow. Separation point (A) and reattachment point (B) as indicated in figure 4 computed on the mesh at $Re = 300$, $H = 0$ and $\beta = 1$.

Code Validation

The outflow domain length was tested to confirm that it is adequately long to ensure that the solutions are insensitive to the effect of the outflow. The primary recirculation bubble length was used as the convergence criterion in a convergence study with a range of the outflow length $20a \leq e - b \leq 100a$. It was found that an outflow length of $e - b = 47a$ is sufficiently long as it yields only a 0.0002% error compared to the longest outflow length studied.

It is observed that the flow separation of the primary recirculation bubble starts from the sharp inner corner of the bend near location A in figure 4. Points of separation and reattachment are identified at location along the horizontal duct walls here

$$\left. \frac{\partial u}{\partial y} \right|_x = 0. \quad (6)$$

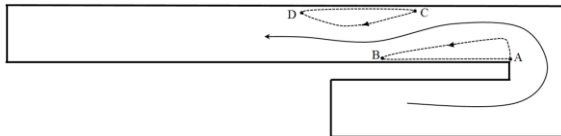


Figure 4: Separation (A and C) and reattachment (B and D) points. Reproduced from Zhang and Poth erat (2013).

The distance between the separation (A and C) and reattachment points (B and D) describe the lengths of the primary and secondary recirculation bubbles, respectively. The code is validated by comparing the primary recirculation bubble length L_{R1}/a obtained in non-MHD flow in the range of $100 \leq Re \leq 700$ in the current study with the results acquired by Zhang and Poth erat (2013) and Chung *et al.* (2003) using regression analysis and only shows discrepancies as small as 2.2% and 0.2%, respectively (Figure 5). The tail of the curves from Zhang and Poth erat (2013) has small discrepancy due to the difference in resolution which leads to a formation of small scale vortices at far downstream in their study.

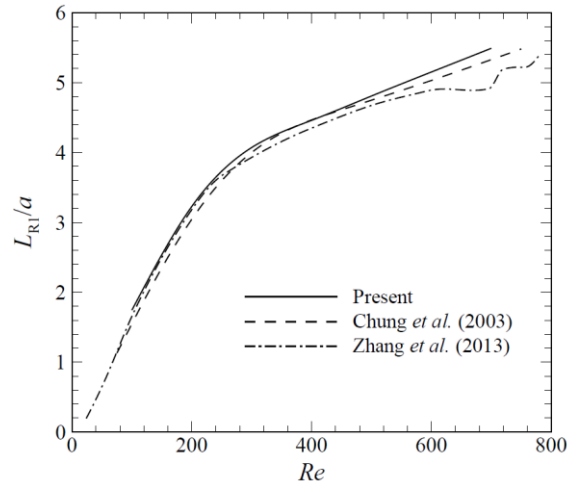


Figure 5: Plot of the first recirculation bubble length (L_{R1}/a) against Reynolds number (Re), comparing the present results to those of Zhang and Poth erat (2013) and Chung *et al.* (2003).

RESULTS

Numerical simulations were conducted at Hartmann friction parameters ranging from $H = 0$ to 500 with increment of 100, and at a range of Reynolds numbers, $1 \leq Re \leq 4000$. Figure 6 shows the significant influence of the strong spanwise magnetic field on the liquid metal flow structure at the downstream part of the sharp bend, especially on the size of the recirculation bubbles. The length of the recirculation bubbles decrease as the strength of the magnetic field increases. This may at least in part be a consequence of the increase momentum in the side wall boundary layers as they become thinner with increasing H as discussed in figure 2. It is apparent that the secondary bubble disappears beyond certain value of H as can be seen from the effect of increasing H in figure 6 and figure 7. The length of the bubbles were calculated by finding the distance between the separation and reattachment point which can be found using equation 6.

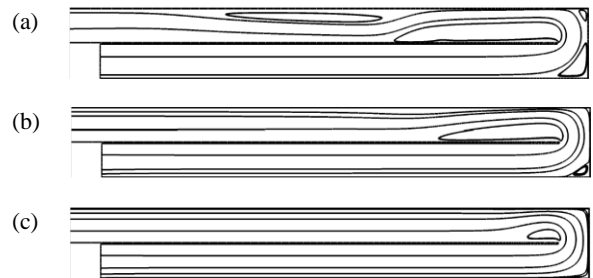


Figure 6: Streamlines of steady flow for $Re = 700$, (a) $H = 0$, (b) $H = 100$ and (c) $H = 500$.

Parameter Space

Figure 7 categorizes the flow in a range of Re with the effect of H into several regimes. The threshold Reynolds numbers for the formation of first and second bubbles captured by the numerical simulations are represented by Re_{R1} and Re_{R2} , respectively. The critical Re at the onset of unsteadiness is denoted by Re_c . The regime below the Re_{R1} does not have any detectable separation bubbles as the magnitude of the adverse pressure gradient behind the

bend is not strong enough to invoke flow separation. The threshold Re for the first bubble to start to form is not significantly affected by the increase of H . However, the appearance of the second bubble is significantly delayed as H is increased. The relationship between Re_{R2} and H for $\beta = 1$ can be approximated by the polynomial equation

$$Re_{R2} = 0.0076H^2 + 5.7725H + 157.25, \quad (7)$$

with coefficient of correlation $R^2 = 0.9974$.

There are two thresholds of Re for the flow to transition to unsteady flow due to hysteretic behaviour in the flow. A stable steady-state solution was preserved by incrementally increasing Reynolds number to an unsteady threshold Re_{c_upper} well above the threshold Re_{c_lower} below which the unsteady solution branch reverts to steady flow with decreasing Reynolds number. These two critical Re are shown in figure 7 with the striped region denoting the range of Re over which hysteretic behaviour was observed. A representative flow within this region is shown in figure 8.

The gap between the Re_{c_upper} and Re_{c_lower} increases as H increased from $H = 0$ to 100 before decreasing as H increased further. The Re_{c_lower} increases consistently with increasing H . At low H , Re_{c_upper} increases rapidly with H , before adopting a more gradual increase between $H \approx 90$ and 300. This is more apparent at $H \geq 317$ where the flow does not have secondary recirculation bubble prior to the transition to unsteady flow.

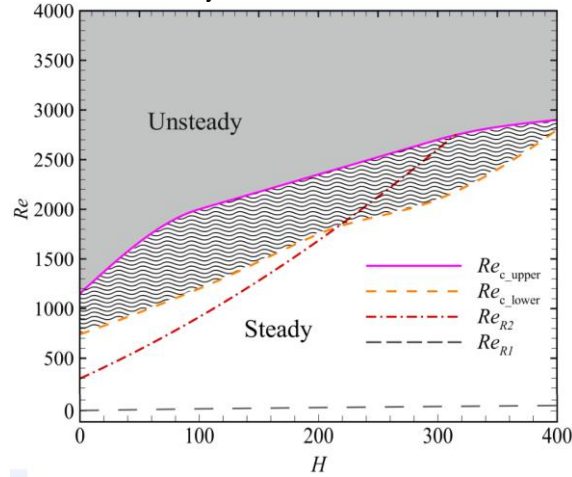


Figure 7: Thresholds of Reynolds number where the first bubble and the second bubble start to appear, (Re_{R1} and Re_{R2} , respectively) and the flow transitioned from steady to unsteady (Re_c) for $\beta=1$, $0 \leq Re \leq 4000$ and $0 \leq H \leq 400$.

Figure 9 shows the magnitude of vorticity for $Re = 1500$ across a range of H . The flow is strongly unsteady when there is no magnetic field effect (Figure 9(a)). As the magnetic field is imposed, the vortices in the downstream duct are dampened due to the effect of the induced force opposing the motion of the flow in the duct. Figure 9(b) shows the dampened vortices in the downstream duct when H is increased to 100. As H increases to 200 and beyond, the flow becomes steady with decreasing size of bubbles when H is increased.

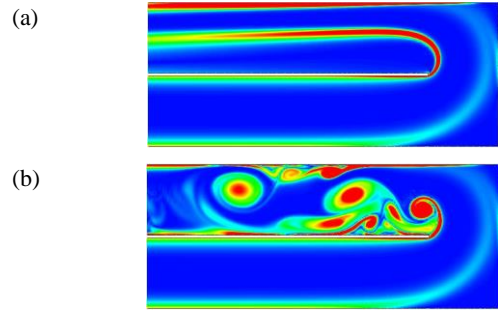


Figure 8: Magnitude of vorticity contours in the hysteresis region with $Re = 2000$, $H = 200$, depicting (a) the steady and (b) unsteady solution branches.

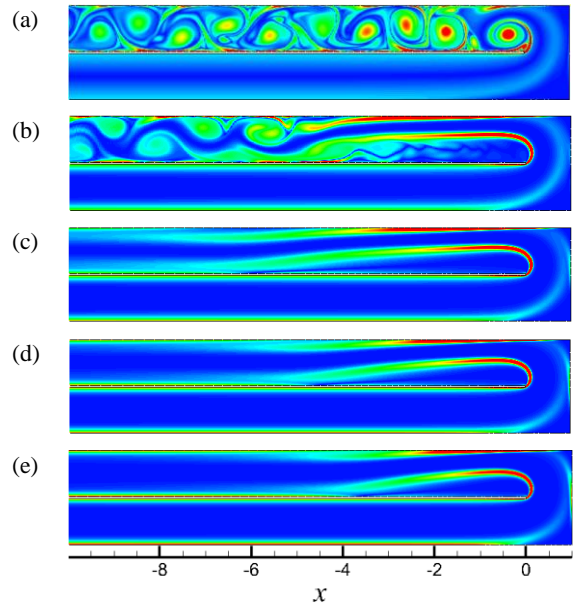


Figure 9: Magnitude of vorticity contours for $Re = 1500$ in unsteady flow regime at (a) $H=0$, (b) $H=100$, and steady-state flow regime at (c) $H=200$, (d) $H=300$, and (e) $H=400$.

The effect of gap ratio on the unsteady flow regime is now considered. From the magnitude of vorticity contours in unsteady flow shown in Figure 10, $\beta = 0.2$ produces very strong vortices behind the sharp bend compared to $\beta = 0.5, 1$ and 2. This smallest gap ratio shows that vorticity from both the inner and outer sides of the gap interact, vorticity from the shear layers is rolled into vortices which initiates unsteady flow immediately behind the bend. The flow at the smaller opening ratio is able to sustain the high magnitude of vorticity further downstream compared to the larger opening ratio. However, the unsteady flow in $\beta = 2$ is able to sustain the vorticity further compared to 1. This might be due to the effective opening ratio for $\beta = 2$ is actually smaller compared to 1 as a consequence of the formation of a large recirculation bubble at the outer wall of the bend. Figure 11(b) demonstrates the presence of the huge recirculation bubble at the outer wall of the bend for $\beta > 1$ which limits the motion of the bulk flow from moving further horizontally, and instead starts to move upward and turns to the outlet earlier than $\beta = 1$. This bubble also narrows the opening for the bulk flow to pass through, acting like a slip wall instead of a non-slip

condition, which sees the bulk flow accelerates at the bend, hence creating a more unstable flow compared to $\beta = 1$.

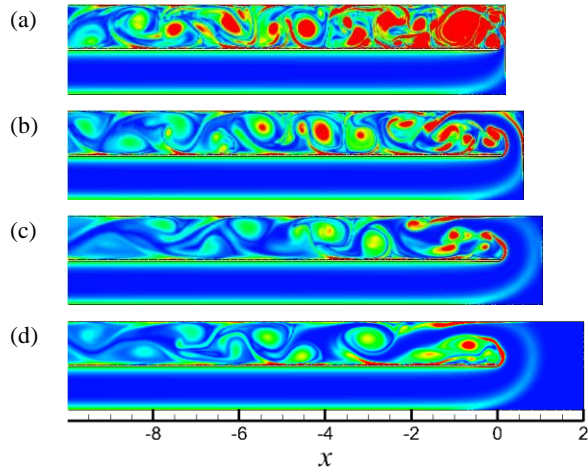


Figure 10: The structure of the unsteady flow at $Re = 1200$ and $H = 100$ for (a) $\beta = 0.2$, (b) $\beta = 0.5$, (c) $\beta = 1$ and (d) $\beta = 2$ initiated from scratch.

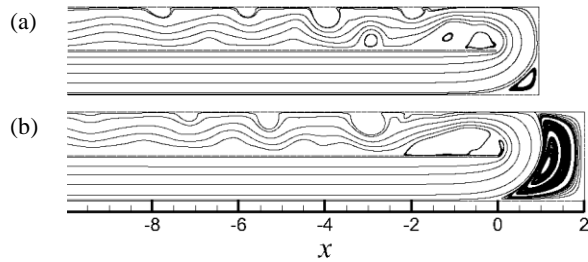


Figure 11: The flow streamlines at $Re = 1200$ and $H = 100$ for (a) $\beta = 1$ and (b) $\beta = 2$.

Recirculation Bubbles

Figure 12 shows the length of the primary recirculation bubble as a function of Re at $\beta = 1$. L_{R1}/a increases linearly with increasing Re for a constant H , and decreases with H when Re is fixed. Apparently when the secondary recirculation bubble starts to form further downstream, the growth of the primary recirculation bubble becomes slower with increasing Re .

An optimization was performed to find the best exponents A , B and C to maximize the coefficient of correlation (R^2) of a linear fit to L_{R1}/a when plotted against $Re^A H^B \beta^C$. The L_{R1}/a data is collected in the range of $Re < Re_{c_upper}$. The optimal exponents were determined to be $A = 0.9568$, $B = -0.648$ and $C = -0.6005$ with $R^2 = 0.9963$. The relationship between the primary recirculation bubble length, Re , H and β is approximated by

$$L_{R1} = 0.1713Re^{0.9568}H^{-0.648}\beta^{-0.6005} - 0.2367 \quad (8)$$

which is shown along with the collapsed data in figure 13.

The collapse of data in equation 8 and figure 13 can be further improved by removing the region where the second bubble exists because the growth of the primary recirculation bubble is highly linear prior to the appearance of the second bubble. By limiting the range to $Re \leq Re_{R2}$, a linear trend line with a better correlation with the data of L_{R1}/a can be obtained. The optimum exponents

are $A = 1.0003$, $B = -0.7483$ and $C = -0.6643$ with improved $R^2 = 0.9991$. These exponents are very similar to the fraction values of 1, $-3/4$ and $-2/3$, respectively. The universal relationship can thus be approximated by

$$L_{R1} = 0.2224ReH^{-3/4}\beta^{-2/3} - 0.2091 \quad (9)$$

which is depicted in figure 14.

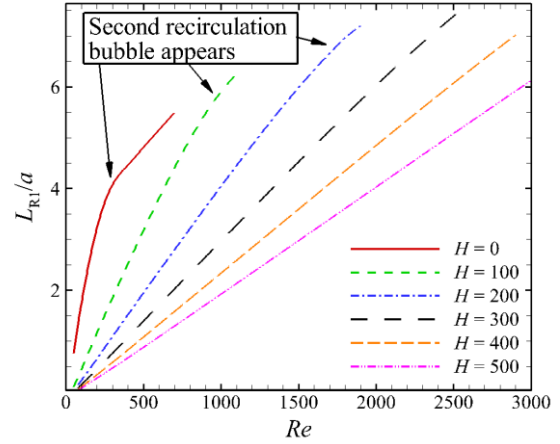


Figure 12: Primary recirculation bubble length in the function of Re for $\beta = 1$, $0 \leq H \leq 500$ and $10 \leq Re \leq 3000$.

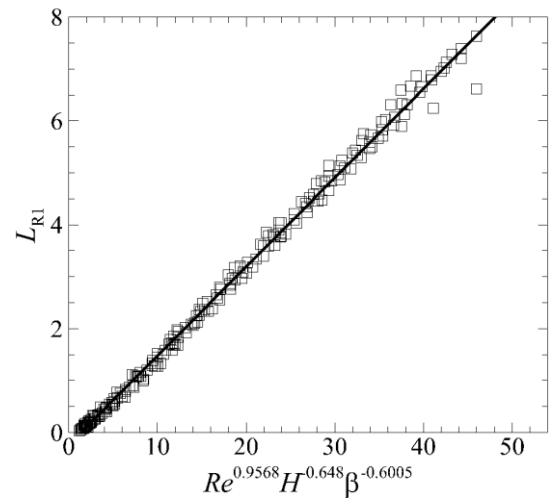


Figure 13: Collapse of primary recirculation bubble over ranges of Hartmann $100 \leq H \leq 500$, $10 \leq Re \leq 3000$ and opening ratio $0.3 \leq \beta \leq 1$ when plotted against $Re^{0.9568}H^{-0.648}\beta^{-0.6005}$.

CONCLUSION

The liquid metal flow past a 180-degree sharp bend under a very strong spanwise homogeneous magnetic field has been studied. Due to the high values of N and H ($N \gg 1$ and $H \gg 1$), the flow can be assumed to be quasi-two-dimensional, thus SM82 model can be applied for the numerical simulations (Sommeria and Moreau, 1982). The recirculation bubbles created from the separation and reattachment flow caused by the abrupt geometry of the sharp bend are damped as H increased due to the

Hartmann braking effect. The thresholds of Re for the formation of primary recirculation bubble and secondary recirculation bubble were delayed as H is increased. The same trend has been seen for the critical Reynolds number for the transition from steady to unsteady flow. The effect of the magnetic field to the structure of the flow for different opening ratio, especially on the thresholds Reynolds number between steady-state and unsteady flow regimes discussed in this study may be very useful in the optimization of heat transfer efficiency for MHD applications.

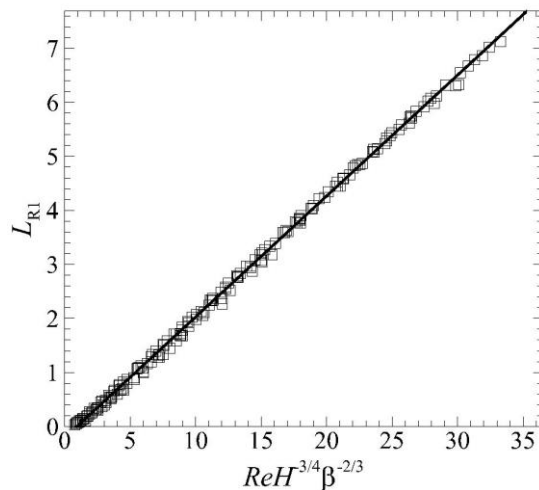


Figure 14: Collapse of primary recirculation bubble over ranges of Hartmann $100 \leq H \leq 500$, $10 \leq Re \leq 2000$ and opening ratio $0.3 \leq \beta \leq 1$ when plotted against $ReH^{3/4}\beta^{-2/3}$. This collapse excludes the regime where the second bubble exists.

ACKNOWLEDGEMENTS

A. M. S. is supported by the Ministry of Education Malaysia and International Islamic University Malaysia. This research was supported by Discovery Grants DP120100153 and DP150102920 from the Australian Research Council, and was undertaken with the assistance of resources from the National Computational Infrastructure (NCI), which is supported by the Australian Government.

REFERENCES

ASTARITA, T. and CARDONE, G., (2000). "Thermofluidynamic analysis of the flow in a sharp 180 turn channel", *Exp. Therm. Fluid Sci.*, **20**(3), 188-200.

BARLEON, L., CASAL, V. and LENHART, L., (1991). "MHD flow in liquid-metal-cooled blankets", *Fusion Eng. Des.*, **14**(3), 401-412.

BARLEON, L., MACK, K. J. and STIEGLITZ, R., (1996). "The MEKKA-facility: A Flexible Tool to Investigate MHD-flow Phenomena", Forschungszentrum Karlsruhe.

BOCCACCINI, L., GIANCARLI, L., JANESCHITZ, G., HERMSMEYER, S., POITEVIN, Y., CARDELLA, A. and DIEGELE, E., (2004). "Materials and design of the European DEMO blankets", *J. Nucl. Mater.*, **329**, 148-155.

CHUNG, Y. M., TUCKER, P. G. and ROYCHOWDHURY, D., (2003). "Unsteady laminar flow

and convective heat transfer in a sharp 180° bend", *Int. J. Heat Fluid Flow*, **24**(1), 67-76.

HAMID, A. H., HUSSAM, W. K., POTHÉRAT, A. and SHEARD, G. J., (2015). "Spatial evolution of a quasi-two-dimensional Kármán vortex street subjected to a strong uniform magnetic field", *Phys. Fluids*, **27**(5), 053602.

HIROTA, M., FUJITA, H., SYUHADA, A., ARAKI, S., YOSHIDA, T. and TANAKA, T., (1999). "Heat/mass transfer characteristics in two-pass smooth channels with a sharp 180-deg turn", *Int. J. Heat Mass Tran.*, **42**(20), 3757-3770.

KIRILLOV, I. R., REED, C. B., BARLEON, L. and MIYAZAKI, K., (1995). "Present understanding of MHD and heat transfer phenomena for liquid metal blankets", *Fusion Eng. Des.*, **27**, 553-569.

LIU, T.-M., CHEN, C.-C., TZENG, Y.-Y. and TSAI, T.-W., (2000). "Non-intrusive measurements of near-wall fluid flow and surface heat transfer in a serpentine passage", *Int. J. Heat Mass Tran.*, **43**(17), 3233-3244.

LIU, T.-M., TZENG, Y.-Y. and CHEN, C.-C. (1998). "Fluid flow in a 180 deg sharp turning duct with different divider thicknesses" *ASME 1998 International Gas Turbine and Aeroengine Congress and Exhibition*, American Society of Mechanical Engineers.

POTHÉRAT, A., SOMMERIA, J. and MOREAU, R., (2000). "An effective two-dimensional model for MHD flows with transverse magnetic field", *J. Fluid Mech.*, **424**, 75-100.

POTHÉRAT, A., SOMMERIA, J. and MOREAU, R., (2005). "Numerical simulations of an effective two-dimensional model for flows with a transverse magnetic field", *J. Fluid Mech.*, **534**, 115-143.

SOMMERIA, J. and MOREAU, R., (1982). "Why, how, and when, MHD turbulence becomes two-dimensional", *J. Fluid Mech.*, **118**, 507-518.

SPARROW, E., KANG, S. and CHUCK, W., (1987). "Relation between the points of flow reattachment and maximum heat transfer for regions of flow separation", *Int. J. Heat Mass Tran.*, **30**(7), 1237-1246.

ZHANG, L. and POTHÉRAT, A., (2013). "Influence of the geometry on the two-and three-dimensional dynamics of the flow in a 180° sharp bend", *Phys. Fluids*, **25**(5), 053605.